Microchimica Acta (2021) 188: 112
https://doi.org/10.1007/s00604-021-04769-2

ORIGINAL PAPER

Electrochemical determination of hantavirus using gold nanoparticle-modified graphene as an electrode material and Cu-based metal-organic framework assisted signal generation

Xu Yiwei[1] · Li Yahui[1] · Tan Weilong[2] · Shi Jiyong[1] · Zou Xiaobo[1] · Zhang Wen[1] · Zhang Xinai[1] · Li Yanxiao[3] · Zhu Changqiang[2] · Ai Lele[2] · Li Hong[2] · Shen Tingting[1]

Received: 1 November 2020 / Accepted: 20 February 2021 / Published online: 6 March 2021

Abstract

An electrochemical biosensor was prepared for nucleic acid-based hantavirus detection using a Cu-based metal-organic framework (CuMOF) as a signal tag. The CuMOF was synthesized by the solvothermal method and then covalently bonded with signal DNA (sDNA) probes. The Au nanoparticles and reduced graphene oxide composite were deposited on the electrode surface by electroreduction as support substrate and was then functionalized with capture DNA (cDNA) probes by self-assembly. Through the complementary base pairing, the target DNA (tDNA) fragment of hantavirus hybridized with the cDNA and the sDNA in a sandwich-type format. The tDNA was detected according to the current signal of the CuMOF catalyzed reaction using *o*-phenylenediamine as redox substrate. The peak current of the biosensor at − 0.55 V increased linearly in proportion to the logarithmic value of the tDNA concentration from 10^{-15} to 10^{-9} mol/L, with a detection limit of 0.74×10^{-15} mol/L. Moreover, the proposed biosensor was successfully applied to detect hantavirus and was able to distinguish hantavirus from other arboviruses.

Keywords Electrochemical biosensor · Metal-organic framework · Peroxidase-like activity · Hantavirus detection

Introduction

Hantavirus (HTV) is a kind of enveloped negative-sense RNA virus, belonging to the Bunyaviridae family [1]. The reservoir species of HTV include rodents, bats, shrews, and moles. The infection normally occurs through close contact with the reservoir species carrying HTV and their excreta. HTV has attracted worldwide attention, because it is the causative agent of human diseases including hemorrhagic fever with renal syndrome and hantavirus pulmonary syndrome [2]. Since the infection is difficult to be early diagnosed by clinical examination and the case fatality rate is up to 60% [3], the effort is essentially focused on HTV detection. In principal, the virus can be detected based on either specific nucleic acid or protein analysis [4]. Because of the thermal instability of proteins, the protein-based methods suffer from limits in application [5]. Contrarily, the nucleic acid-based methods have attracted more and more attentions, because nucleic acid is more thermostable than protein [6]. Besides, the specific nucleic acid can be amplified from the genome by polymerase chain reaction (PCR) utilizing a species-specific primer. Recently, numerous sensor techniques have been developed for nucleic acid analysis, such as colorimetric, fluorescence, Raman spectroscopy, and electrochemical [7]. Among these analysis methods, electrochemical biosensor has been recognized as a promising candidate for nucleic acid detection, because of its low cost, simple operation, and fast response, which can be miniaturized for point-of-care test [8].

Sandwich hybridization assay is very popular in electrochemical sensing for nucleic acid detection. In sandwich hybridization assay, horseradish peroxidase (HRP) is frequently

✉ Tan Weilong
njcdc@163.com

✉ Zou Xiaobo
zou_xiaobo@ujs.edu.cn

[1] School of Food and Biological Engineering, Jiangsu University, Zhenjiang 212013, China

[2] Department of Vector Control, Huadong Research Institute for Medicine and Biotechnics, Nanjing 210002, China

[3] Centre for instrumental analysis, Jiangsu University, Zhenjiang 212013, China

used as a signal tag to provide an electrochemical signal for readout, due to its catalytic capacity for the hydrogen peroxide-mediated reaction [9]. However, the catalytic activity of HRP is easy to be affected by the experiment condition, because of the fragile nature of the enzyme [10]. Metal-organic framework (MOF) as a kind of crystalline porous materials constructed by assembling metal ions with multidentate organic ligands via coordination bonds has been proved to possess peroxidase-like catalytic activity recently [11]. In comparison to HRP, MOF is more suitable for sensing applications owing to unique advantages such as good stability, large surface area, and high porosity [12]. Based on the peroxidase-like activity, many MOF materials have been employed as a signal tag to fabricate electrochemical sensors, exhibiting satisfactory sensing performance [13].

In the electrochemical analysis, a large sensing interface would allow the immobilization of more capture probes, contributing to increasing the sensitivity. Graphene has believed to be a promising support material for the electrochemical sensor, owing to its large surface area, excellent electric conductivity, and strong mechanical strength [14]. However, graphene sheets tend to stack and self-aggregate due to the strong π interaction, leading to a negative effect in electrochemical sensing [15]. The introduction of metal nanomaterials to graphene sheets is an efficient approach to prevent the formation of the agglomerate. Among the large number of metal nanomaterials, Au nanoparticles (AuNPs) are very popular because of the fascinating electrical and chemical properties [16]. Moreover, AuNPs are readily functionalized with biomolecules due to the good biocompatibility [17]. Consequently, the combination of AuNPs and reduced graphene oxide (RGO) has attracted much attention in the development of the novel electrochemical sensor.

The electrochemical biosensors for hantavirus detection have been reported previously [18–20]. These biosensors are based on antigen-antibody reactions for hantavirus detection. However, the specific antibody can only be detected from 7 to 12 days of hantavirus infection, which is just after or during the first hantavirus cardiopulmonary syndrome [20]. Therefore, hantavirus diagnosis through antigen-antibody reaction is not fast enough, which is not conducive to the disease treatment. Alternatively, the detection of hantavirus-specific nucleic acid can be a good approach for early diagnosis. As far as we know, the electrochemical biosensor based on specific nucleic acid for hantavirus detection has not been reported yet. In this work, a nucleic acid-based electrochemical biosensor is proposed for hantavirus detection using AuNPs-RGO composite as supporting substrate and Cu-based MOF (CuMOF) as a signal tag. The AuNPs-RGO composite was deposited on the electrode surface by electroreduction. Capture DNA (cDNA) probes were immobilized on AuNPs by Au-S bond. The CuMOF was synthesized by the solvothermal method using 2-aminoterephthalic acid as linker and Cu as a node and then covalently bonded with signal DNA (sDNA) probes. Based on complementary base pairing, the target DNA (tDNA) fragment of HTV hybridized with the AuNPs-RGO surface-immobilized cDNA and the CuMOF-labeled sDNA in a sandwich-type format. Through the hybridization reaction, CuMOF was attached to the sensing interface. Owing to the peroxidase-like activity, CuMOF was able to catalyze the oxidation of *o*-phenylenediamine (*o*-PD). The electrochemical signal of the oxidized *o*-PD product (*o*-PDox) was recorded for the quantitative analysis of the tDNA.

Materials and methods

Reagents and instruments

Chloroauric acid hydrate ($HAuCl_4 \cdot 4H_2O$), copper nitrate trihydrate ($Cu(NO_3)_2 \cdot 3H_2O$), polyvinyl pyrrolidone (PVP), N,N-dimethylformamide (DMF), tris(2-chloroethyl) phosphate (TCEP), hydrogen peroxide (H_2O_2, 30 wt.%), tris(hydroxymethyl)aminomethane (Tris), hydrogen chloride (HCl), ethylenediamine tetraacetic acid (EDTA), 6-mercapto-1-hexanol (MCH), sulfuric acid (H_2SO_4), potassium chloride (KCl), sodium chloride (NaCl), sodium carbonate (Na_2CO_3), sodium hydrogen carbonate ($NaHCO_3$), disodium hydrogen phosphate dodecahydrate ($Na_2HPO_4 \cdot 12H_2O$), sodium dihydrogen phosphate dihydrate ($NaH_2PO_4 \cdot 2H_2O$), potassium ferrocyanide trihydrate ($K_4Fe(CN)_6 \cdot 3H_2O$), potassium ferricyanide ($K_3Fe(CN)_6$), 2-aminoterephthalic acid (NH_2-BDC), and glutaraldehyde and *o*-PD were purchased from Sinopharm Chemical Reagent Co., Ltd. Bovine serum albumin (BSA) was purchased from Sigma-Aldrich Co., Ltd. Graphene oxide (GO) was obtained from XFNANO Materials Tech Co., Ltd. The oligonucleotides were synthesized by Sangon Biotechnology Co., Ltd. and purified by high-performance liquid chromatography. The sequences of the oligonucleotides were shown in Table S1.

The electrochemical measurements were performed by a CHI 660D workstation (Shanghai CH Instruments, China) with a conventional three-electrode system including a glassy carbon electrode (GCE) as a working electrode, a platinum wire electrode as the auxiliary electrode, and an Ag/AgCl (saturated KCl) electrode as a reference electrode. Scanning electron microscope (SEM) image was taken by a JSM-7800F field emission SEM instrument (JEOL, Japan). Transmission electron microscopy (TEM) image was taken by a JEM-2100 high-resolution TEM instrument (JEOL, Japan). Energy-dispersive X-ray (EDX) spectrum and mapping were collected by a GENESIS 2000 XM spectrometer (EDAX, America). The X-ray diffraction (XRD) pattern was obtained by a D8 ADVANCE diffractometer (Bruker, Germany). The X-ray photoelectron (XPS) spectrum was collected by a Nexsa spectrometer (Thermo Fisher Scientific, America). Fourier

transform infrared (FT-IR) spectrum was collected on a Nicolet is50 FT-IR spectrometer (Thermo Fisher Scientific, America). UV-Vis spectrum was recorded on a Cary 500 UV-Vis spectrometer (Varian Comp, USA). Pure water was produced by a Millipore Milli-Q water purification system.

Synthesis of CuMOF-sDNA

CuMOF was synthesized by a solvothermal method according to the reported literature [12]. The synthesis process was described in the electronic supporting material.

The sDNA was linked to CuMOF by covalent bonds. Firstly, 5 mg CuMOF was dispersed in 5 mL of 2.5% glutaraldehyde and then reacted for 2 h. The CuMOF was collected by centrifugation, washed, and dispersed in 5 mL of 0.01 mol/L Tris-HCl buffer (pH = 7.4). After that, 10 μL of 0.1 mmol/L sDNA (with an amino at the 3′-end) was added into the dispersion and then reacted for 24 h. The product was collected by centrifugation, blocked with 1% BSA, and washed with water. Finally, the obtained CuMOF-sDNA was dispersed in 10 mL of 0.01 mol/L Tris-HCl buffer solution (pH = 7.4) containing 1 mmol/L EDTA and 0.05 mol/L NaCl.

Preparation of MCH/cDNA/AuNPs-RGO/GCE

The AuNPs-RGO composite was deposited on the GCE surface by cyclic voltammetry (CV). Before modification, the GCE surface was cleaned as the following procedures: polished with 0.30 μm and 0.05 μm alumina slurries respectively; sonicated in acetone and water successively; and immediately dried with nitrogen. After that, CV was performed between 0.6 V and − 1.6 V at 25 mV/s using the polished GCE in an electrolyte containing 1 mg/mL GO, 0.5 mmol/L $AuCl_4^-$, and 0.1 mol/L carbonate buffer solution (pH = 9). In this process, $AuCl_4^-$ and GO in electrolytes were reduced to AuNPs-RGO composite on the GCE surface. Finally, the AuNPs-RGO/GCE was activated in 0.5 mol/L H_2SO_4 by CV in the potential range of 0.2–1.4 V at 100 mV/s.

The cDNA was immobilized on AuNPs-RGO/GCE surface by self-assembly. Firstly, 0.1 mmol/L cDNA stock solution was mixed with 10 mmol/L TCEP and reacted for 60 min to cleave the disulfide bond. Then, the cDNA stock solution was diluted to 10 μmol/L by 0.01 mol/L Tris-HCl buffer solution (pH = 7.4) containing 1 mmol/L EDTA. After that, 8 μL of 10 μmol/L cDNA was dropped on AuNPs-RGO/GCE and stored at 4 °C for 10 h. The thiolated cDNA assembled on AuNPs-RGO/GCE by Au-S bond. Subsequently, the electrode surface was blocked with 1 mmol/L MCH at 4 °C for 1 h. The immobilization of MCH blocked the nonspecific adsorption of the gold surface, which contributed to reducing the background signal.

Electrochemical measurement

The electroactive areas of GCE and AuNPs-RGO/GCE were measured by CV (potential range between 0.6 V and − 0.2 V, scan rates of 10, 25, 50, 75, 100, 150, and 200 mV/s) in an electrolyte containing 5 mmol/L $[Fe(CN_6)]^{3-/4-}$ and 0.1 mol/L KCl.

The stepwise preparation of MCH/cDNA/AuNPs-RGO/GCE was studied by electrochemical impedance spectroscopy (EIS) in an electrolyte containing 5 mmol/L $[Fe(CN_6)]^{3-/4-}$ and 0.1 mol/L KCl. The EIS was conducted in the frequency range of 10^{-2}–10^5 Hz, with a sinusoidal voltage amplitude of 5 mV.

The electrochemical response towards tDNA was obtained by differential pulse voltammetry (DPV). Firstly, the hybridization buffer was prepared using 0.01 mol/L Tris-HCl (pH = 7.4), 1 mmol/L EDTA, and 0.05 mol/L NaCl. The MCH/cDNA/AuNPs-RGO/GCE was immersed in a hybridization buffer with different concentrations of tDNA. After incubation at 37 °C for 60 min, the tDNA hybridized with cDNA through the complementary base pairing. Subsequently, the electrode was incubated in CuMOF-sDNA dispersion at 37 °C for 90 min. Through the hybridization between sDNA and tDNA, CuMOF was attached to the sensing interface. Finally, the current signal of the biosensor was measured by DPV in a nitrogen-saturated electrolyte containing 0.1 mol/L PBS (pH = 7), 10 mmol/L *o*-PD, and 8 mmol/L H_2O_2. The nitrogen-saturated electrolyte was prepared by deaeration thoroughly with highly pure nitrogen for 10 min and maintained in a nitrogen atmosphere before use (Scheme 1).

Virus sample preparation

Virus samples of HTV, dengue virus (DENV), Japanese encephalitis virus (JEV), and Zika virus (ZIKV) were provided

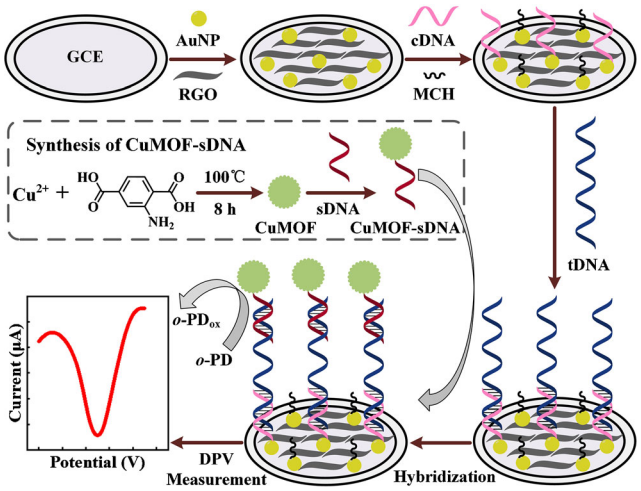

Scheme 1 Schematic diagram for the preparation of MCH/cDNA/AuNPs-RGO/GCE and the procedure of tDNA detection

by Huadong Research Institute for Medicine and Biotechnics. Firstly, 140-μL sample was taken into a 1.5-mL centrifuge tube, and the viral RNA was extracted from the sample using TaKaRa MiniBEST Universal RNA Extraction Kit according to the protocol of the manufacturer. Then, the extracted RNA was converted into DNA by reverse transcription using PrimeScript TMRT reagent Kit with gDNA Eraser RR047A. After that, PCR was performed to amplify the tDNA fragment using the reverse transcription product as a template and the specifically designed primers. The PCR parameters were as follows: denaturation at 94 °C for 3 min, followed by 30 cycles of amplification at 94 °C for 30 s, at 55 °C for 30 s, at 72 °C for 30 s, and a final extension at 72 °C for 4 min. Finally, the PCR products were diluted with 1 mL of hybridization buffer, denatured by heating at 95 °C for 5 min, and freezing in an ice bath for 1 min to obtain the single-stranded tDNA fragment for electrochemical analysis [21].

The electrochemical analysis was performed as follows. Firstly, MCH/cDNA/AuNPs-RGO/GCE was immersed in the hybridization buffer containing the PCR products and incubated at 37 °C for 60 min. After that, the electrode was incubated in CuMOF-sDNA dispersion at 37 °C for 90 min. Finally, the voltammogram was recorded by DPV at the potential range from − 0.4 to − 0.7 V in a nitrogen-saturated electrolyte containing 0.1 mol/L PBS (pH = 7), 10 mmol/L *o*-PD, and 8 mmol/L H_2O_2.

Results and discussion

Characterization of CuMOF

The morphology of CuMOF was investigated by SEM and TEM. From Fig. 1a–c, CuMOF was observed as a spherical particle. The diameter of the CuMOF particle was in the range of 260–400 nm. As shown in Fig. 1d, the EDX mapping revealed the uniform distribution of Cu, O, N, and C elements in CuMOF particle. The crystal structure of CuMOF was analyzed by XRD. As shown in Fig. S1, the XRD pattern revealed that the prepared CuMOF had good crystallinity, and its characteristic diffraction peaks were highly similar to the theoretical calculation and the reported results in previous literature [22]. The XPS spectrum of CuMOF was shown in Fig. S2. The binding energy peaks at 284.7 eV, 399.7 eV, and 531.6 eV were ascribed to C 1s, N 1s, and O 1s respectively. The peaks at 934.3 eV and 954.1 eV were assigned to Cu $2p_{3/2}$ and Cu $2p_{1/2}$ of CuO, and the peaks at 943.9 eV and 962.5 eV belonged to the open $3d^9$ shell of Cu^{2+} [13]. The XPS spectrum indicated the element composition of CuMOF. The FT-IR spectra of CuMOF and NH_2-BDC were exhibited in Fig. 1e. The FT-IR spectrum of NH_2-BDC exhibited two distinct peaks at 3507 cm^{-1} and 3393 cm^{-1} respectively, due to the asymmetric and symmetric stretching vibrations of the -NH_2 group [23]. These peaks shifted to 3477 cm^{-1} and 3362 cm^{-1} in the FT-IR spectrum of CuMOF, owing to the formation of intra-framework hydrogen bonding of amine group with an electron-donating oxygen from the carboxylic group [24]. It indicated that the -NH_2 group of NH_2-BDC was retained in CuMOF. The stretching vibration peak of -OH was observed at 2990 cm^{-1} in the FT-IR spectrum of NH_2-BDC. However, this peak was disappeared in the FT-IR spectrum of CuMOF, which was resulted from the coordination interaction between -COOH of NH_2-BDC and Cu^{2+} in CuMOF. The above proofs demonstrated the successful synthesis of CuMOF.

The catalytic activity of CuMOF was investigated by the chromogenic reaction. The UV-Vis adsorption spectra and typical photographs were shown in Fig. 1f and Fig. S3. The *o*-PD and H_2O_2 mixture was colorless and transparent, and no absorption peak was found in the UV-Vis spectrum. In addition of 10 mg/L CuMOF to the *o*-PD and H_2O_2 mixture and incubation for 10 min, the color of the solution turned to yellow, and a distinct absorption peak at 410 nm was observed in the UV-Vis spectrum. The dramatic color changes resulted from the oxidation of colorless *o*-PD to yellow *o*-PDox [25]. The above result indicated that CuMOF had the catalytic capacity to oxidize *o*-PD and could be used to obtain an electrochemical signal.

Characterization of AuNPs-RGO composite

The deposition of AuNPs-RGO composite on GCE surface was performed by CV. In Fig. S4a, a cathodic peak was observed at about − 1.50 V. It was ascribed to the irreversible electroreduction of GO [26]. The reduction current intensity was enhanced with continuous CV scanning, indicating the successive deposition of RGO with a large specific surface on GCE. Because of the presence of metallic precursor in the electrolyte, $AuCl_4^-$ was reduced to yield AuNPs under low potential during CV scanning. After deposition, the electrode was activated in 0.5 mol/L H_2SO_4. In Fig. S4b, the anodic peak at 1.19 V and 1.37 V was related to the Au oxidation, and the cathodic peak at 0.88 V was derived from the regeneration of metallic Au [27]. The above results indicated that AuNPs-RGO composite was formed on the electrode surface.

The morphology of the deposited AuNPs-RGO composite was characterized by SEM. As shown in Fig. 2a–c, RGO exhibited a wrinkled structure, and AuNPs were observed as bright spots. This morphology rendered AuNPs-RGO composite an effective support substrate to immobilize cDNA. The element component of the AuNPs-RGO composite was investigated by EDX. In Fig. 2d, there were characteristic peaks of Au and C elements in the EDX spectrum, indicating the existence of these elements in the AuNPs-RGO composite. The SEM images and EDX spectrum confirmed that the AuNPs-RGO composite was successfully modified on the GCE surface.

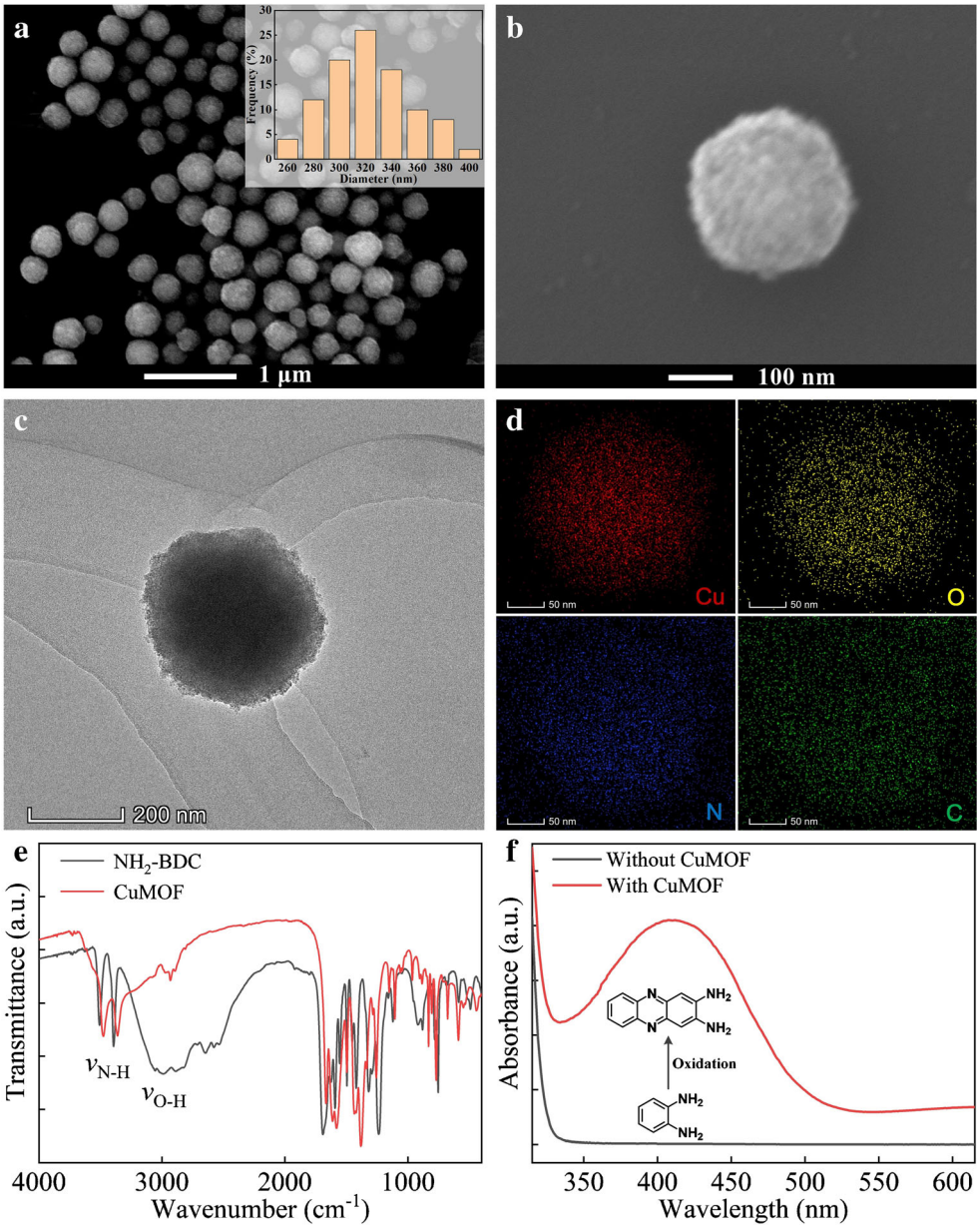

Fig. 1 **a**, **b** SEM images, **c** TEM image, and **d** EDX mapping of CuMOF, **e** FT-IR spectra of CuMOF and 2-aminoterephthalic acid, **f** UV-Vis absorption spectra of *o*-PD and H_2O_2 mixtures (10 mmol/L *o*-PD and 8 mmol/L H_2O_2 in 0.1 mol/L pH = 7 PBS) incubated with and without CuMOF

Electrochemical characterization

The electroactive areas of GCE before and after deposition of AuNPs-RGO composite were evaluated by CV at different scan rates. As shown in Fig. 3a, b, the peak current increased linearly with the square root of scan rate, which was typical for a reversible diffusion-controlled reaction [28]. The slop of the calibration curve was obtained for the calculation of the electroactive area. According to the Randles-Sevcik equation, the electroactive area of bare GCE was calculated to be 6.14 ± 0.27 mm^2. The electroactive area of GCE was smaller than its geometrical area (7.07 mm^2). It might be caused by some inactive sites on the GCE surface. The electroactive area of AuNPs-RGO/GCE was 18.0 ± 1.03 mm^2 by the calculation. It was about 3-fold larger than that of bare GCE. Because the three-dimensional structure of AuNPs-RGO composite enlarged the specific area on the sensing interface. Therefore, the deposited AuNPs-RGO composite could provide a rather larger surface for the immobilization of cDNA, which contributed to improving the electrochemical signal.

The layer-by-layer steps of the sensor preparation were investigated by EIS. As shown in Fig. 3c, the EIS data were presented as Nyquist plots that were fitted by a Randles equivalent circuit. The equivalent circuit included the resistance of the solution (R_s), the resistance of electron transfer (R_{et}), the double-layer capacitance (C_{dl}), and the Warburg impedance (Z_w). The Nyquist plot involved two portions: the semicircle at high frequencies and the straight at low frequencies. The

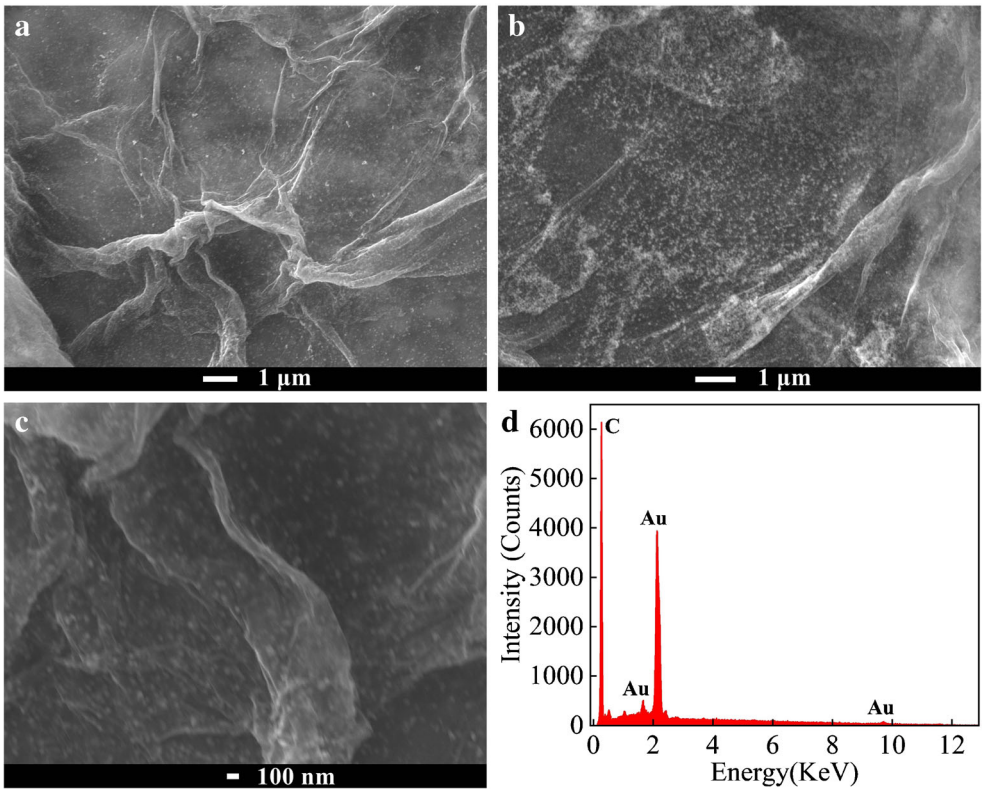

Fig. 2 **a**–**c** SEM images and **d** EDX spectrum of AuNPs-RGO composite

semicircle was related to the electron transfer kinetics at the interface between electrode and electrolyte. The R_{et} value could be evaluated by the semicircular diameter. The R_{et} of bare GCE was estimated to be 320 ± 19 Ω. Compared with the GCE, the R_{et} of AuNPs-RGO/GCE decreased to 190 ± 14 Ω, because AuNPs promoted the electron transfer on the electrochemical surface [29]. After the cDNA assembled on AuNPs, the R_{et} significantly increased to 1050 ± 65 Ω. Because the phosphate backbone of DNA was electronegative in a neutral environment, it had an electrostatic repulsion to the negatively charged $[Fe(CN)_6]^{3-/4-}$ and hindered the electron transfer reaction [30]. After the treatment with MCH, the R_{et} further increased to 1420 ± 73 Ω. It was because the MCH monolayer blocked the gold surface and retarded the electron transfer reaction [31]. After hybridization with tDNA, the R_{et} increased to 1540 ± 78 Ω. When CuMOF-cDNA immobilized on electrode surface, a great increase of R_{et} was obtained (R_{et} = 5040 ± 262 Ω), mainly due to the poor conductivity of CuMOF. The above results confirmed the successful preparation of all layer-by-layer steps.

The DPV responses from all layer-by-layer steps of the biosensor preparation were shown in Fig. 3d. The bare GCE exhibited a small peak at about − 0.55 V, which was attributed to the slow oxidation of *o*-PD. After the electrodeposition of AuNPs-RGO, the peak was improved, mainly due to the good electrical conductivity of AuNPs-RGO. When cDNA is immobilized on the electrode surface, the peak decreased slightly because the cDNA molecules hindered the redox reaction on the sensing interface. After the immobilization of MCH and tDNA, the peak further decreased, because some nonspecific sites were blocked. When CuMOF-sDNA was immobilized on the electrode surface by complementary base pairing, the peak was significantly improved, because the immobilized CuMOF on the sensing interface catalyzed oxidation of *o*-PD. These different DPV responses further confirmed the successful preparation of the biosensor.

The electrochemical mechanism for tDNA detection could be explained as follows: In the absence of tDNA, the biosensor of MCH/cDNA/AuNPs-RGO/GCE exhibited a small current in an electrolyte containing *o*-PD and H_2O_2 mixtures, because of the slow oxidation of *o*-PD without a catalyst. In the presence of tDNA, the tDNA hybridized with the AuNPs-RGO surface-immobilized cDNA at 3′-end and the CuMOF labeled sDNA at 5′-end in a sandwich-type format. Owing to the peroxidase-like activity, the immobilized CuMOF on the sensing interface could catalyze the oxidation of *o*-PD, leading to a significantly improved current. Therefore, the tDNA could be quantified by the difference of the current signal.

Analytical performance of the biosensor

The analytical performance of the biosensor was seriously influenced by the experimental conditions. Therefore, the key experiment parameters were optimized, including the hybridization time between cDNA and tDNA, the hybridization time between tDNA and sDNA, and the

concentrations of redox substrates (*o*-PD and H_2O_2). As shown in Fig. S5, the optimal experimental parameters were as follows: 60 min of hybridization between cDNA and tDNA, 90 min of hybridization between tDNA and sDNA, 10 mmol/L of *o*-PD, and 8 mmol/L of H_2O_2. Under the optimal conditions, the biosensor was employed to analyze tDNA with different concentrations. As shown in Fig. 4, the current intensity at − 0.55 V was improved as tDNA concentration increased because more tDNA fragments were captured by cDNA probes with the increased tDNA concentration. Subsequently, more CuMOF nanoparticles were attached to the sensing surface by the hybridization between tDNA and sDNA. Therefore, more *o*-PD oxidation products were obtained due to the CuMOF catalyzed reaction, leading to the enhanced current signal. The reduction current improved in proportion to the logarithm of the tDNA concentration from 10^{-15} to 10^{-9} mol/L. The regression equation was $I_p = -2.751\ gC - 55.87$ ($R^2 = 0.988$); I_p was the peak current [μA]; C was the concentration of tDNA [mol/L]. Based on signal-to-noise characteristics (S/N = 3), the detection limit was calculated to be 0.74×10^{-15} mol/L. Compared with previously reported biosensors [32–35], the proposed biosensor exhibited a lower detection limit, as well as a wider detection range (Table 1). The good analysis performance of the biosensor was attributed to the synergistic of AuNPs-RGO composite and CuMOF: the AuNPs-RGO composite as supporting substrate, not only provided a large surface to immobilize cDNA but also promoted the electron transfer on sensing interface; thanks to the peroxidase-like activity, CuMOF as signal tag produced sensitive electrochemical signal.

To study the repeatability, a fresh biosensor was used for tDNA detection and then treated with 50 mmol/L NaOH for 5 min to break the DNA duplexes on the electrode surface. This process was repeated for several times, and DPV responses for 1 nmol/L tDNA and blank sample from each analysis were recorded (Fig. S6a). It was found that the relative standard deviation (RSD) of peak currents were 4.19% for tDNA and 2.93% for blank sample 4 times of repeated analysis, indicating good repeatability. It suggested that the cDNA probes were perfectly maintained on the electrode surface and the DNA duplexes were broken during the regeneration process. After 4 times of repeated analysis, a noticeable decrement of peak current was found, which was mainly due to the damage of the sensing interface. Therefore, 4 cycles of the regeneration were suggested for the proposed biosensor. In

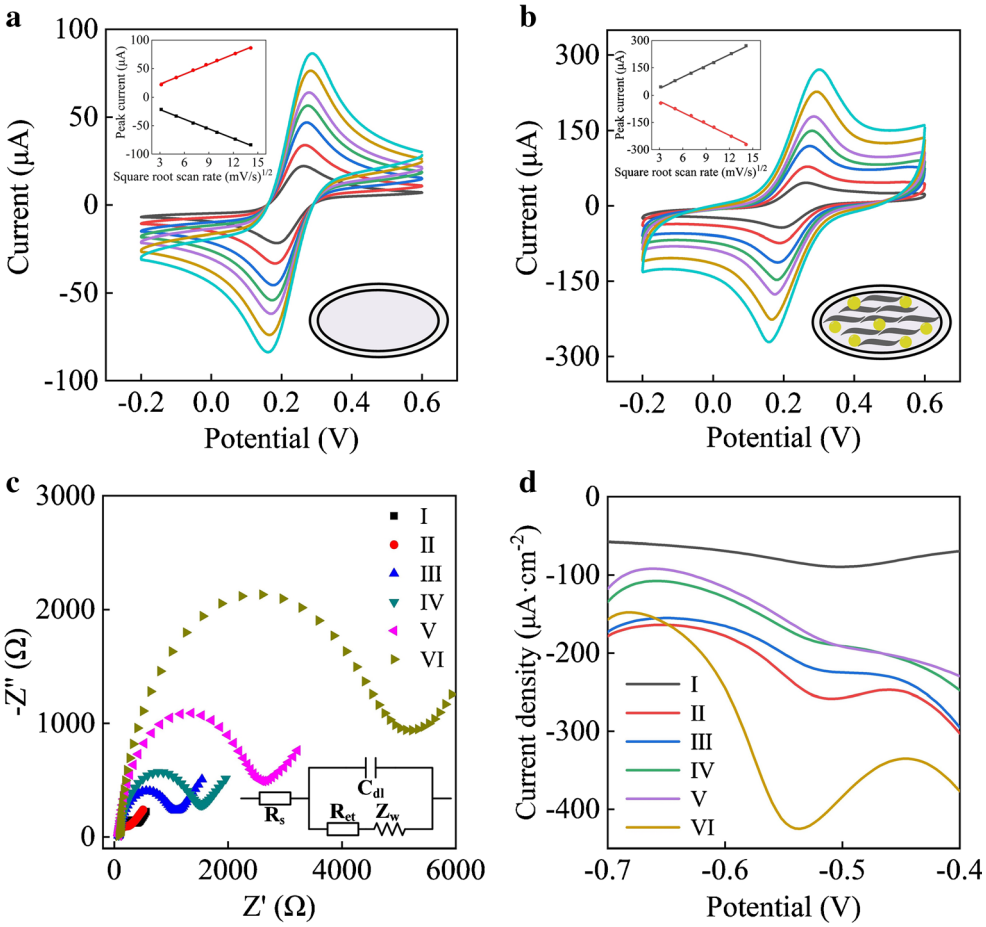

Fig. 3 CV responses of **a** GCE and **b** AuNPs-RGO/GCE at 10, 25, 50, 75, 100, 150, and 200 mV/s in 5 mmol/L $[Fe(CN_6)]^{3-/4-}$; **c** Nyquist plots and **d** DPV responses of (I) GCE, (II) AuNPs-RGO/GCE, (III) cDNA/AuNPs-RGO/GCE, (IV) MCH/cDNA/AuNPs-RGO/GCE and then hybridized with (V) tDNA and (VI) CuMOF-sDNA successively

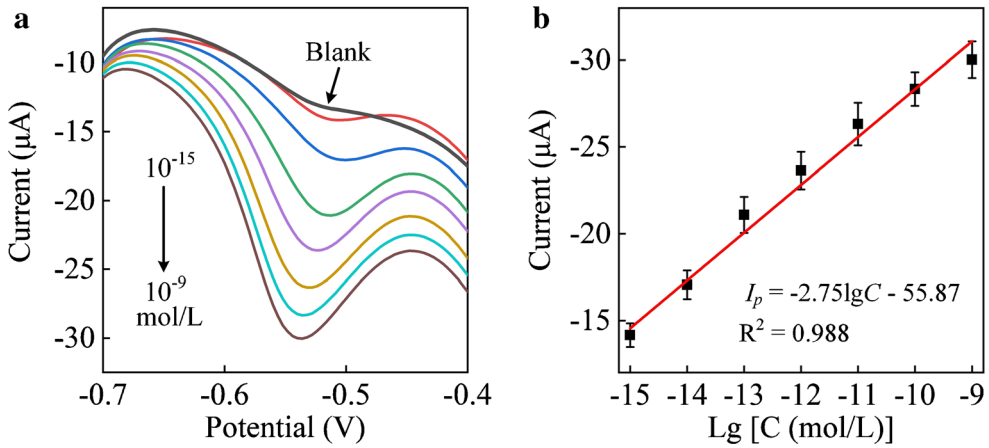

Fig. 4 **a** DPV responses for tDNA with different concentrations and **b** the corresponding calibration curve

order to investigate the reproducibility, CuMOF-sDNA suspension as well as five electrodes of MCH/cDNA/AuNPs-RGO/GCE were prepared and then employed to detect tDNA. As shown in Fig. S6b, these biosensors produced similar electrochemical responses towards 1 nmol/L tDNA. The relative standard deviation (RSD) of the peak current from different biosensors was 4.45%, exhibiting good reproducibility. In addition, the storage lifetime of the biosensor was studied. The CuMOF-sDNA suspension and MCH/cDNA/AuNPs-RGO/GCE were stored in a refrigerator at 4 °C, and the DPV response for 1 nmol/L tDNA was recorded every day. After 7 days, the biosensor still retained 91.82% of its original peak current (Fig. S6c), indicating that the storage stability of the biosensor was acceptable. According to the above results, the storage lifetime of the proposed biosensor was 7 days.

Hantavirus detection

The biosensor was applied to detect real virus samples. Before electrochemical analysis, the genome of HTV was extracted using a kit and converted into DNA by reverse transcription; then, the tDNA fragments were produced by PCR amplification using the reverse transcription product as a template and the specifically designed primers. The DPV responses of the biosensor were exhibited in Fig. 5a. The sample without HTV did not cause the improvement of the current signal compared with blank control, because of the absence of tDNA fragment in PCR products. In the case of the HTV sample, the obtained current signal showed a remarkable improvement, owing to the presence of tDNA fragment in PCR products. Moreover, the PCR products from the HTV sample were studied by electrophoresis. As shown in the inset of Fig. 5a, a bright band was appeared between 100 pb and 250 pb, confirming that the tDNA fragment was obtained from the HTV sample after reverse transcription and PCR amplification. In addition, the selectivity of the biosensor was evaluated by analysis of other arboviruses including DENV, JEV, and ZIKV (Fig. 5b). In the analysis of individual arboviruses, only HTV triggered an obvious improvement of the current signal, while other viruses did not exhibit a noteworthy current change, indicating that the biosensor could specifically recognize HTV. In the analysis of the binary mixtures, the biosensor responses were close to that of HTV, indicating that other arboviruses did not affect the HTV detection. The above results demonstrated that the proposed biosensor was able to detect HTV selectively.

Table 1 Electrochemical biosensors for target DNA detection

Sensing strategy	Analytical technique	Linear range (mol/L)	Detection limit (mol/L)	Refs.
Direct hybridization with hairpin DNA probe/gold electrode	EIS	10^{-12}–10^{-9}	1.71×10^{-13}	[32]
Sandwich hybridization with thiolated DNA capture probe/gold nanoparticles/reduced graphene oxide/screen printed carbon electrode and biotinylated DNA detection probe	DPV	10^{-14}-2×10^{-12}	5×10^{-15}	[33]
Direct hybridization with DNA probe/sulfonamide/GCE	EIS	10^{-14}–10^{-8}	2×10^{-14}	[34]
Direct hybridization with cross-shaped DNA origami/-chitosan/gold electrode	DPV	10^{-13}–10^{-8}	7.98×10^{-14}	[35]
Sandwich hybridization with MCH/cDNA/AuNPs-RGO/GCE and CuMOF-sDNA	DPV	10^{-15}–10^{-9}	0.74×10^{-15}	This work

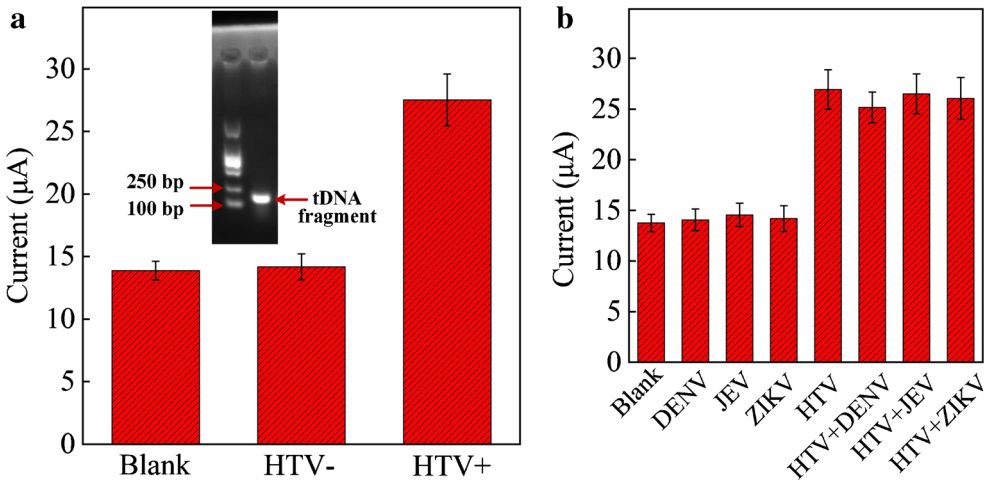

Fig. 5 **a** Biosensor responses for blank control and the samples with and without HTV, **b** biosensor responses for different viruses

Conclusion

An electrochemical biosensor was prepared using CuMOF as a signal tag for HTV detection. The CuMOF was synthesized by the solvothermal method and covalently bonded with sDNA. The AuNPs-RGO composite was deposited on the electrode surface by electroreduction as support substrate and then was functionalized with cDNA by self-assembly. In the presence of tDNA fragment, the immobilized cDNA on AuNPs-RGO composite and the labeled sDNA by CuMOF hybridized with tDNA at 3′-end and 5′-end respectively in a sandwich-type format. Benefiting from the catalytic activity of CuMOF and the large electroactive area of AuNPs-RGO composite, the biosensor exhibited a sensitive electrochemical response towards tDNA. Moreover, the biosensor was successfully applied to detect HTV and was able to distinguish HTV from other arboviruses. Owing to the high sensitivity and selectivity, the proposed biosensor has great potential in the diagnosis of HTV infection. However, several pretreatment processes including RNA extraction, reverse transcription, and PCR are necessary to obtain hantavirus-specific nucleic acid before HTV sample analysis, which are complicated and time-consuming. In order to improve the current method, ongoing work is focused on shortening the sample processing time.

Supplementary Information The online version contains supplementary material available at https://doi.org/10.1007/s00604-021-04769-2.

Funding This study was supported by the Development Fund of Key Laboratory of Virology Institute of Wuhan University (2020KF003), Medical Research Topics of Jiangsu Provincial Health Planning Commission (H2019015), China Postdoctoral Science Foundation (2019 M661760), National Key Research and Development Program of China (2018YFD0400800).

Declarations

Conflict of interest The authors declare no competing interests.

References

1. Jiang H, Zheng X, Wang L, Du H, Wang P, Bai X (2017) Hantavirus infection: a global zoonotic challenge. Virol Sin 32(1):32–43. https://doi.org/10.1007/s12250-016-3899-x
2. Papa A (2012) Dobrava-Belgrade virus: phylogeny, epidemiology, disease. Antivir Res 95(2):104–117. https://doi.org/10.1016/j.antiviral.2012.05.011
3. Stanojevic M, Cirkovic V, Siljic M, Gligic A, Stamenkovic G (2019) Molecular characterization of Dobrava-Belgrade hantavirus in Serbia, 2007–2011. J Infect Public Health 12(5):645–649. https://doi.org/10.1016/j.jiph.2019.02.021
4. Batule BS, Seok Y, Kim M-G (2020) Paper-based nucleic acid testing system for simple and early diagnosis of mosquito-borne RNA viruses from human serum. Biosens Bioelectron 151: 111998. https://doi.org/10.1016/j.bios.2019.111998
5. Mansouri M, Khalilzadeh B, Barzegari A, Shoeibi S, Isildak S, Bargahi N, Omidi Y, Dastmalchi S, Rashidi M-R (2020) Design a highly specific sequence for electrochemical evaluation of meat adulteration in cooked sausages. Biosens Bioelectron 150:111916. https://doi.org/10.1016/j.bios.2019.111916
6. Lai RY, Lagally ET, Lee SH, Soh HT, Plaxco KW, Heeger AJ (2006) Rapid, sequence-specific detection of unpurified PCR amplicons via a reusable, electrochemical sensor. Proc Natl Acad Sci U S A 103(11):4017–4021. https://doi.org/10.1073/pnas.0511325103
7. Wu W, Yu C, Wang Q, Zhao F, He H, Liu C, Yang Q (2020) Research advances of DNA aptasensors for foodborne pathogen detection. Crit Rev Food Sci Nutr 60(14):2353–2368. https://doi.org/10.1080/10408398.2019.1636763
8. Valipour A, Roushani M (2017) A glassy carbon immunoelectrode modified with vanadium oxide nanobelts for ultrasensitive voltammetric determination of the core antigen of hepatitis C virus. Microchim Acta 184(11):4477–4483. https://doi.org/10.1007/s00604-017-2449-z
9. Nasir M, Nawaz MH, Latif U, Yaqub M, Hayat A, Rahim A (2017) An overview on enzyme-mimicking nanomaterials for use in electrochemical and optical assays. Microchim Acta 184(2):323–342. https://doi.org/10.1007/s00604-016-2036-8

10. Zhang D, Zhang J, Zhang R, Shi H, Guo Y, Guo X, Li S, Yuan B (2015) 3D porous metal-organic framework as an efficient electrocatalyst for nonenzymatic sensing application. Talanta 144: 1176–1181. https://doi.org/10.1016/j.talanta.2015.07.091
11. Qian X, Tan S, Li Z, Qu Q, Li L, Yang L (2020) A robust host-guest interaction controlled probe immobilization strategy for the ultra-sensitive detection of HBV DNA using hollow HP5–Au/CoS nanobox as biosensing platform. Biosens Bioelectron 153: 112051. https://doi.org/10.1016/j.bios.2020.112051
12. Wang S, Deng W, Yang L, Tan Y, Xie Q, Yao S (2017) Copper-based metal–organic framework nanoparticles with peroxidase-like activity for sensitive colorimetric detection of Staphylococcus aureus. ACS Appl Mater Interfaces 9(29):24440–24445. https://doi.org/10.1021/acsami.7b07307
13. Shen W-J, Zhuo Y, Chai Y-Q, Yuan R (2015) Cu-based metal–organic frameworks as a catalyst to construct a ratiometric electrochemical aptasensor for sensitive lipopolysaccharide detection. Anal Chem 87(22):11345–11352. https://doi.org/10.1021/acs.analchem.5b02694
14. Coroş M, Pruneanu S, Stefan-van Staden R-I (2020) Review—recent progress in the graphene-based electrochemical sensors and biosensors. J Electrochem Soc 167(3):037528. https://doi.org/10.1149/2.0282003JES
15. Liu J, Fu S, Yuan B, Li Y, Deng Z (2010) Toward a universal "adhesive nanosheet" for the assembly of multiple nanoparticles based on a protein-induced reduction/decoration of graphene oxide. J Am Chem Soc 132(21):7279–7281. https://doi.org/10.1021/ja100938r
16. Layqah LA, Eissa S (2019) An electrochemical immunosensor for the corona virus associated with the Middle East respiratory syndrome using an array of gold nanoparticle-modified carbon electrodes. Microchim Acta 186(4):224. https://doi.org/10.1007/s00604-019-3345-5
17. Karimizefreh A, Mahyari FA, VaezJalali M, Mohammadpour R, Sasanpour P (2017) Impedimetic biosensor for the DNA of the human papilloma virus based on the use of gold nanosheets. Microchim Acta 184(6):1729–1737. https://doi.org/10.1007/s00604-017-2173-8
18. Vetcha S, Abdel-Hamid I, Atanasov P, Ivnitski D, Wilkins E, Hjelle B (2000) Portable immunosensor for the fast amperometric detection of anti-hantavirus antibodies. Electroanalysis 12(13):1034–1038. https://doi.org/10.1002/1521-4109(200009)12:13<1034::AID-ELAN1034>3.0.CO;2-L
19. Gogola JL, Martins G, Caetano FR, Ricciardi-Jorge T, Duarte dos Santos CN, Marcolino-Junior LH, Bergamini MF (2019) Label-free electrochemical immunosensor for quick detection of anti-hantavirus antibody. J Electroanal Chem 842:140–145. https://doi.org/10.1016/j.jelechem.2019.04.066
20. Martins G, Gogola JL, Caetano FR, Kalinke C, Jorge TR, Santos CND, Bergamini MF, Marcolino-Junior LH (2019) Quick electrochemical immunoassay for hantavirus detection based on biochar platform. Talanta 204:163–171. https://doi.org/10.1016/j.talanta.2019.05.101
21. Sousa JB, Ramos-Jesus J, Silva LC, Pereira C, de-los-Santos-Álvarez N, Fonseca RAS, Miranda-Castro R, Delerue-Matos C, Santos Júnior JR, Barroso MF (2020) Fe3O4@Au nanoparticles-based magnetoplatform for the HMGA maize endogenous gene electrochemical genosensing. Talanta 206:120220. https://doi.org/10.1016/j.talanta.2019.120220
22. Khan J, Iqbal N, Asghar A, Noor T (2019) Novel amine functionalized metal organic framework synthesis for enhanced carbon dioxide capture. Mater Res Express 6(10):105539. https://doi.org/10.1088/2053-1591/ab3ff8
23. Zhao M, Deng K, He L, Liu Y, Li G, Zhao H, Tang Z (2014) Core–Shell palladium nanoparticle@metal–organic frameworks as multifunctional catalysts for cascade reactions. J Am Chem Soc 136(5): 1738–1741. https://doi.org/10.1021/ja411468e
24. Ming F, Hou J, Huo D, Zhou J, Yang M, Shen C, Zhang S, Hou C (2019) Copper-based metal–organic framework nanoparticles for sensitive fluorescence detection of ferric ions. Anal Methods 11(34):4382–4389. https://doi.org/10.1039/C9AY01093A
25. Fornera S, Walde P (2010) Spectrophotometric quantification of horseradish peroxidase with o-phenylenediamine. Anal Biochem 407(2):293–295. https://doi.org/10.1016/j.ab.2010.07.034
26. Liu C, Wang K, Luo S, Tang Y, Chen L (2011) Direct electrodeposition of graphene enabling the one-step synthesis of graphene–metal nanocomposite films. Small 7(9):1203–1206. https://doi.org/10.1002/smll.201002340
27. Sukeri A, Saravia LPH, Bertotti M (2015) A facile electrochemical approach to fabricate a nanoporous gold film electrode and its electrocatalytic activity towards dissolved oxygen reduction. Phys Chem Chem Phys 17(43):28510–28514. https://doi.org/10.1039/C5CP05220C
28. Määttänen A, Vanamo U, Ihalainen P, Pulkkinen P, Tenhu H, Bobacka J, Peltonen J (2013) A low-cost paper-based inkjet-printed platform for electrochemical analyses. Sens Actuators B: Chem 177:153–162. https://doi.org/10.1016/j.snb.2012.10.113
29. Miao P, Tang Y, Wang L (2017) DNA modified Fe3O4@Au magnetic nanoparticles as selective probes for simultaneous detection of heavy metal ions. ACS Appl Mater Interfaces 9(4):3940–3947. https://doi.org/10.1021/acsami.6b14247
30. Rodriguez MC, Kawde A-N, Wang J (2005) Aptamer biosensor for label-free impedance spectroscopy detection of proteins based on recognition-induced switching of the surface charge. Chem Commun 34:4267–4269. https://doi.org/10.1039/B506571B
31. Fau M, Kowalczyk A, Olejnik P, Nowicka AM (2011) Tight and uniform layer of covalently bound aminoethylophenyl groups perpendicular to gold surface for attachment of biomolecules. Anal Chem 83(24):9281–9288. https://doi.org/10.1021/ac201794m
32. Cheng D, Zhang Y, Wen D, Guo Z, Yang H, Liu Y, Kong J (2019) Hairpin probes based click polymerization for label-free electrochemical detection of human T-lymphotropic virus types II. Anal Chim Acta 1059:86–93. https://doi.org/10.1016/j.aca.2019.01.027
33. Zouari M, Campuzano S, Pingarrón JM, Raouafi N (2020) Femtomolar direct voltammetric determination of circulating miRNAs in sera of cancer patients using an enzymeless biosensor. Anal Chim Acta 1104:188–198. https://doi.org/10.1016/j.aca.2020.01.016
34. Smith DA, Newbury LJ, Drago G, Bowen T, Redman JE (2017) Electrochemical detection of urinary microRNAs via sulfonamide-bound antisense hybridisation. Sens Actuators B: Chem 253:335–341. https://doi.org/10.1016/j.snb.2017.06.069
35. Han S, Liu WY, Yang S, Wang RS (2019) Facile and label-free electrochemical biosensors for microRNA detection based on DNA origami nanostructures. ACS Omega 4(6):11025–11031. https://doi.org/10.1021/acsomega.9b01166